Hamedan University of Technology
Iranian Association of Electrical and Electronics Engineers

Sustainable Energy and Artificial Intelligence

Online ISSN: 3060-8015

Journal Homepage: www.enai.hut.ac.ir

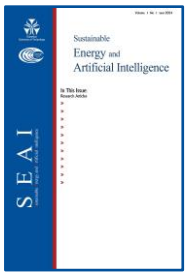

Investigation of Performance Improvement in a Solar Air Heater Equipped with Impinging Jets: A Three-Dimensional Numerical Simulation

Mehdi Ashja[1], Ghanbar Ali Sheikhzadeh[1*], Abolfazl Fattahi[1], Najmeh Hajialigol[2*]

[1] *Faculty of Mechanical Engineering, University of Kashan, Kashan, Iran*
[2] *Department of Mechanical Engineering, Hamedan University of Technology, Hamedan, Iran*
* *Corresponding Authors: sheikhz@kashanu.ac.ir & n.hajialigol@hut.ac.ir*

Article Info

Article type:
Original Article

Article history:
Received 2024-10-09;
Revised 2024-11-07;
Accepted 2024-11-17.

How to cite this article:
Ashja, M., Sheikhzadeh, G. A., Fattahi, A. and Hajialigol, N. (2025). Investigation of Performance Improvement in a Solar Air Heater Equipped with Impinging Jets: A Three-Dimensional Numerical Simulation. *Sustainable Energy and Artificial Intelligence*, *1*(1), 51-66. DOI: 10.61186/seai.2410-1013

Abstract

With the continuous advancement of human civilization, the demand for energy has significantly increased, leading to a heightened need for energy resources. Effectively harnessing solar energy, as one of the most promising sources of energy, is crucial today. Among various applications, solar water heaters have gained widespread adoption, prompting researchers to focus on enhancing their efficiency. This study investigates the use of impinging jets to improve the performance of solar water heaters, numerically, to examine the impact of impinging jets positioned at the absorber plate. A total of 160 configurations were analyzed, assessing the effects of Reynolds number, turbulence intensity, jet diameter, and jet height on the Nusselt number. Operating within a Reynolds number range of 10,000 to 25,000, the results indicate that the PEC increases up to sixfold, while the Nusselt number rise as much as ninefold compared to conventional heaters without impinging jets. The highest cooling effect on the absorber plate, associated with an increase in the Nusselt number, is observed at a Reynolds number of 25,000, achieving a Nusselt number of 495.6. Furthermore, increasing the jet height to half the height of the cooling channel yielded significant performance improvements.

***Keywords*:** Solar Water Heater; Impinging Jets; Numerical Simulation; Hydraulic-Thermal Performance.

Nomenclature

T_{ESS} (s)	The time constant related to the ESS	T_{ESS} (s)	The time constant related to the ESS
a	The longitudinal distance of the jets (m)	b	The lateral distance of the jets (m)
D_h	Channel hydraulic diameter (m)	c_p	Specific thermal capacity (J/kgK)
D_j	Jet diameter (m)	H_j	Jet height (m)
H	Channel height (m)	k	Turbulent kinetic energy (m^2/s^2)
$\dot{q}$	Heat flux (W/m^2)	Nu	Nusselt number
f	Friction factor	P	Pressure (Pa)
PEC	Performance evaluation criterion	Pr	Prandtl number
T	Static temperature (K)	T_W	Wall temperature (K)
T_{inlet}	Flow inlet temperature (K)	V	Velocity magnitude (m/s)
W	Channel width (m)		

Greek symbols			
λ	Thermal conductivity (W/mK)	μ	Dynamic viscosity (N.s/m^2)
ε	Turbulent dissipation rate (m^2/s^3)	ρ	Density (kg/m^3)

1. Introduction

Extensive studies have been conducted on impinging jets in solar heaters, and this topic has garnered even more attention from researchers due to its impressive efficiency [1]. In recent years, there has been a noticeable increase in research focused on impinging jets. Recent advancements in the design of solar heaters have shown significant promise [2,3]. The impact of jets on a corrugated absorber plate has been demonstrated to be an effective method for enhancing heat transfer rates compared to jets impacting flat solar heaters, as explored by Aboghrara et al. [4]. They conducted experiments to determine the influence of mass flow rate on the outlet temperature of solar heaters, concluding that increased disturbance beneath a calm layer leads to greater turbulence in the air and, ultimately, an enhanced heat transfer rate. Comparisons between smooth and corrugated surfaces, under varying airflow rates and solar radiation levels, indicate that the average thermal performance can improve by up to 14%. Nadda et al. [5] conducted an experimental study on impinging jets in solar water heaters with protruding obstacles, reporting optimal values for the relative height ratio, relative step ratio, relative width ratio, and arc angle at 1.0, 9.50, 5.5, and 55 degrees, respectively. They also developed correlations for the Nusselt number and pressure drop coefficient based on their experimental results.

Numerous studies have been conducted on various jet configurations using air as the working fluid in photovoltaic thermal collectors, leading to enhanced electrical and thermal performance. Increased heat transfer is associated with higher friction losses within the fluid flow channel, and both factors depend on the geometric configuration and the Reynolds number of the operating flow [6,7]. Typically, the nozzle jet is commonly turbulent and characterized by a uniform velocity profile [8]. However, as the distance from the nozzle increases, the momentum exchange between the jet and the surrounding environment causes the boundary layer within the jet to expand, preserving the internal potential energy at the outlet velocity [9]. Downstream of the potential core, the velocity profile across the jet's cross-section becomes non-uniform, with the maximum centerline velocity decreasing as the distance from the nozzle increases [10].

Heat transfer effects under a single-axis symmetrical jet for both normal and oblique impact angles were studied by Ichimiya [11] to determine the effects of angled impinging jets. A similar study using two-dimensional jets, normal jets, and varying target distances was conducted by Lin et al. [12], whose experiments demonstrated an increase in the heat transfer coefficient from the heated surface. The heat transfer distribution from tangentially arranged impinging jets in a triangular duct was studied by Huang et al. [13]. To investigate the highest heat transfer rates, average loss coefficient, and average heat transfer, three types of outlet orientations were considered for precise heat transfer coefficient measurements, and the triangular duct with two openings was analyzed along with the relationship between average wall heat transfer, Nusselt number, and pressure drop in a triangular duct developed in Ref. [13]. Chauhan and Thakur [14] conducted an experimental study within a Reynolds number range of 3800 to 16,000, examining airflow through channels that impinge on the absorber surface of a solar heater. They considered the effects of Reynolds number and geometric parameters, such as jet diameter, on heat transfer and friction coefficient. Their study revealed that the high heat transfer coefficient was attributed to the thin boundary layers created by the jets in proximity to the heat transfer surface. While impinging jets induce greater turbulence in the fluid, they ultimately contribute to improved solar water heater performance. Zukowski [15] investigated the thermal characteristics and fluid flow of a solar heater equipped with micro-jets, reporting an energy conversion efficiency ranging from 60% to 90%. Yadav and Saini [16] performed numerical investigations to assess the thermal and friction characteristics of a solar water heater with an impinging jet. They examined the effect of air mass flow rate on the heat transfer surface and studied the impact of dimensionless variables, such as jet diameter ratio and jet height ratio, on heat transfer and friction coefficient within a Reynolds number range of 3500 to 17,500.

The heat transfer characteristics for linear and irregular arrangements of circular air jets with the crossflow were investigated by Metzger and Kind [17], in which ten rows of impinging jets were studied experimentally. They found that the local Nusselt number varied periodically for the first ten rows, with the Nusselt number at the highest impact differing. Furthermore, the local Nusselt

number in the cavities was different from the Nusselt number at the midpoint of the heat transfer surface and between the two cavities. Ingole and Sundaram [18] conducted an experimental study to examine the heat transfer characteristics of inclined jets within the Reynolds number range of 2000 to 20,000. They also recommended equations for the average Nusselt number for inclined air jets in cooling applications. Nayak and Singh [19] studied the effect of the geometry of the impinging air jet on the solar heater, considering various parameters including flow rate and depth ratio within a Reynolds number range of 2700 to 6900. Their findings demonstrated that this configuration exhibited higher efficiency compared to conventional solar heaters. The relationship between the Nusselt number and friction coefficient was also presented.

Rajaseenivasan et al. [20] conducted experiments to investigate the thermal performance of air impinging jets at various angles of attack in a solar heater. The results indicated that the optimal hole diameter was 5mm, and further reductions in hole diameter led to increased pressure drop in the solar water heater. The average Nusselt number increased with airflow rate, resulting in enhanced heat transfer from the absorber plate to the air. It was also reported that the maximum thermal coefficient of 2.19 was achieved with a mass flow rate of 0.016kg/s, a nozzle diameter of 5mm, and an angle of attack of 30 degrees. Lam and Prakash [21] conducted numerical experiments using an array of air jets with an optimized cooling system design, yielding values for heat transfer and entropy. Singh et al. [22] conducted experimental and numerical investigations to evaluate the thermal performance using circular impinging jets to enhance solar heater efficiency. They presented the effects of geometric and flow variables for two solar heater models: one with a turbulent environment and one without. Their research yielded significant results showing improved thermal performance through the use of circular jet impingement. Furthermore, the results indicated that the generated vortices enhance the heating of air and the storage of thermal energy within the porous medium. Zhu et al. [23] examined the transient heat transfer characteristics of an array of jets impinging on a flat surface at high temperatures, focusing on close jet-to-surface distances. They considered variations in transient heat transfer characteristics at different jet height-to-diameter ratios and the inclusion of reverse flow nozzles on the nozzle plate. For a fixed flow rate, when the distance between the jets remains constant, the heat transfer rate is effectively improved with an increase in nozzle diameter, resulting in a uniform enhancement of internal heat transfer. Moreover, incorporating reverse flow nozzles in this region significantly boosts heat transfer rates.

Kumar et al. [24] performed an experimental study to develop new correlations for heat transfer and pressure drop influenced by the presence of conical ring obstacles in a solar heater with impinging jets. They considered geometric variables, Nusselt number ratios, and friction coefficients for circular air jets with internal conical ring obstacles. Their study reported that the multiple vortices generated by the obstacles and circular impinging jets lead to significant turbulence. This flow pattern results in a relatively longer flow path within the circular air jets passing through the channel space, causing substantial turbulence between the wall and the main flow region, which significantly enhances heat transfer. Alomar et al. [25] compared the performance of a traditional v-corrugated absorber plate with a modified design in a solar air heater having jet flows. The modified plate demonstrated superior thermal efficiency, achieving up to 14.5% higher efficiency than the traditional design.

Yadav et al. [26] studied the potential of improving the heat transfer and overall efficiency of a solar air heater through the use of jet impingement on the absorber plate. The results revealed a significant enhancement in thermal-hydraulic performance with the use of jet impingement, achieving a maximum thermo-hydraulic performance parameter of 4.12. This optimal performance was observed at specific values of jet pitch ratio and jet angle ratio at a Reynolds number of 7500. Hai et al. [27] investigated the possibility of enhancing the efficiency of solar air heaters by positioning inclined impinging jets on their surfaces. Two different nozzle configurations, parallel and crossing, were examined, numerically to analyze the impact of various geometrical and operational factors, such as jet size, angle, spacing, flow rate, and velocity ratio. The heat transfer rate increased by up to 4.26 times compared to a standard solar air heater. Increasing the spacing between jets both horizontally and vertically led to improved heat transfer with minimal increase in friction. Almeshaal et al. [28] explored the potential of improving solar air heater performance by combining artificial roughness elements (conical rings) with jet impingement. The results demonstrated that this innovative configuration

significantly outperformed traditional solar air heaters, particularly at lower Reynolds numbers. The enhanced design achieved maximum energy and thermohydraulic efficiencies of 81.4% and 77.4%, respectively, surpassing conventional single-pass and parallel-pass jet impingement systems by 15.1% and 4.1%.

Harikrishnan et al. [29] conducted an in-depth exergetic analysis of a solar air heater with and without impinging air jets. The study aimed to evaluate the exergy losses and identify the primary factors contributing to the system's inefficiency. The maximum thermo-hydraulic efficiency of 84.86% was achieved at a mass flow rate of 0.06kg/s with specific geometric parameters. The analysis revealed that the predominant source of exergy loss in both configurations was due to the temperature difference between the sun and the solar heater surface, accounting for approximately 70% of the total exergy losses. Elwekeel et al. [30] experimentally studied the influence of jet shapes and absorber plate spacing on the heat transfer and pressure drop characteristics of solar air collectors. The experiments were conducted at heat fluxes of 900W/m² and 1000W/m² with Reynolds numbers ranging from 3000 to 19000. The results demonstrated that circular jets significantly outperformed square and triangular jets in terms of heat transfer efficiency. The Nusselt number for circular jets was observed to be 11.64% and 18.94% higher compared to square and triangular jets, respectively. The optimal THP values were obtained at a ratio of absorber plate spacing to jet diameter of 3.3, with circular and triangular jets achieving THP values of 0.96 and 1.04, respectively.

The research conducted thus far has highlighted several computational studies on solar heaters equipped with impinging jets, addressing various parameters. However, previous studies have largely overlooked the specific impact of jet height and diameter ratios on the performance of solar heaters across different configurations. This study uniquely investigates these parameters using a numerical approach, which represents a significant advancement in the understanding of solar heater performance. By comparing and validating the results against previously published numerical and experimental findings, this research aims to identify optimal configurations for solar heaters that utilize impinging jets to maximize heat transfer while effectively managing hydraulic losses. Notably, this investigation focuses on a higher Reynolds number range and introduces previously unexplored values for jet height and diameter ratios. Collectively, these elements underscore the innovative contributions of the present study and fill critical gaps in the current understanding of solar heater performance. Enhancing the efficiency of solar heaters can lead to significant reductions in energy consumption and costs in residential and industrial applications. By optimizing design parameters, the current findings can inform the development of more effective solar heating systems, contributing to increased adoption of renewable energy technologies and supporting sustainability goals.

2. Mathematical Formulation

2-1. Geometry Description

The geometry of the problem involves a cubic channel equipped with impinging jets installed beneath an absorber plate. This setup consists of a simple channel with a total of 98 impinging jets arranged in 14 columns and 7 rows, responsible for fluid entry. As shown in Fig. 1a, the channel has an outlet at one end, and the absorber plate (the heated surface) is positioned above the channel. The walls are modeled as smooth surfaces. The channel length (L), width (W), and height (H) are 150mm, 150mm, and 22mm, respectively. These dimensions are adapted from the study by Yadav and Saini [16], maintaining the scale ratio while reducing the overall dimensions to improve computational efficiency. Fig. 1b provides a detailed view of the channel and the impinging jets, along with a symmetry plane marked at the center of the geometry. All dimensions are listed in Table 1. The jets are modeled as cylindrical with a constant cross-section.

Due to the symmetry of the geometry and the boundary conditions of the problem, only half of the model has been solved numerically, which enhances the computational speed. Thus, a symmetry plane is utilized in the center of the geometry, as shown in Fig. 1b. Additionally, the impinging jets are positioned at a distance from the walls to prevent fluid interaction with the sidewalls and to minimize any potential increase in the friction coefficient.

Table 1. The values of the geometrical variables

Geometrical variables	Values (mm)
Jet length (H_j)	0-11
Jet diameter (D_j)	3-6
Longitudinal distance of jets (a)	10
Lateral distance of jets (b)	10
The jets distance from the lateral wall (Y)	15
The jets distance from the longitudinal wall (X)	15

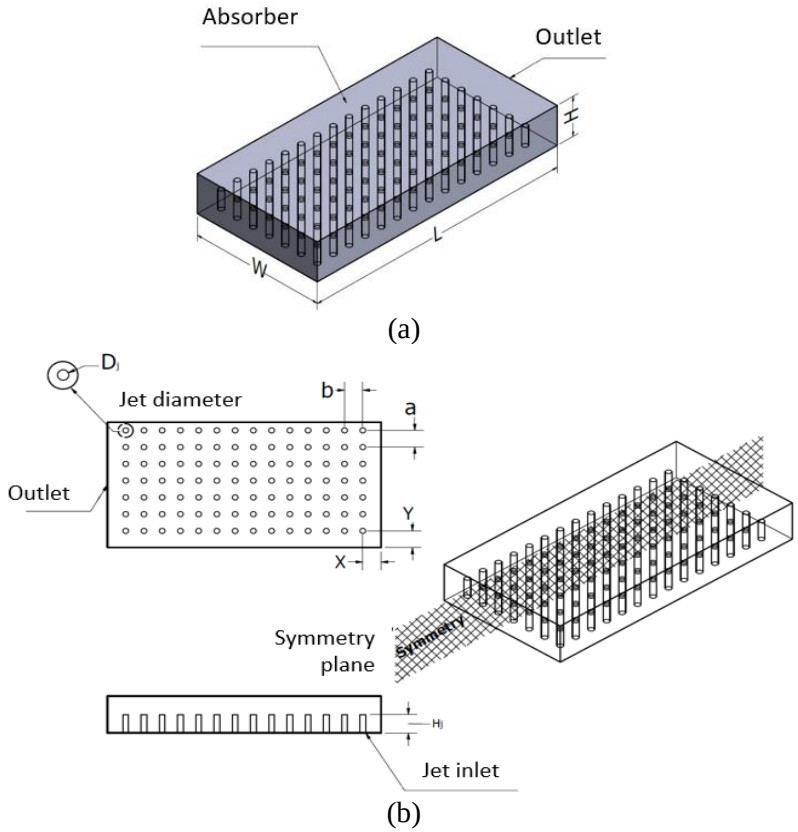

Fig. 1. (a) The overview of the solar heater geometry studied and (b) The isometric, top and lateral view of the geometry

2-2. Governing Equations/Parameters and Assumptions

The governing equations for solving the thermal-hydrodynamic field of the problem are utilized. The continuity, momentum, and energy equations for the three-dimensional solution domain in Cartesian coordinates are presented below for this study. The governing equations are specifically chosen to address the complex fluid dynamics and heat transfer phenomena that occur in these systems. These equations effectively model the high shear rates and localized heat transfer characteristics typical of impinging jets, which are essential for accurately predicting thermal performance. This connection underscores the appropriateness of the mathematical formulation in tackling the unique challenges presented by this application. The following equation represents the continuity equation,

$$\frac{\partial u_i}{\partial x_i} = 0 \tag{1}$$

where u denotes velocity, x represents coordinates, and i is an arbitrary index. The momentum equations reads as

$$\frac{\partial}{\partial x_i}\left(\rho u_i u_j\right) = -\frac{\partial p}{\partial x_i} + \frac{\partial}{\partial x_j}\left[\mu\left(\frac{\partial(\rho u_{\mathrm{i}})}{\partial x_i} + \frac{\partial(\rho u_{\mathrm{i}})}{\partial x_i}\right)\right] + \frac{\partial}{\partial x_j}\left(-\overline{\rho u_i u_j}\right) \tag{2}$$

where j is an arbitrary index, ρ is the fluid density, and μ is the fluid dynamic viscosity. Following this, the energy equation for the fluid is provided as

$$\frac{\partial(u_i T)}{\partial x_i} = \rho\,\frac{\partial}{\partial x_i}\left(\lambda\frac{\partial T}{\partial x_i}\right) + \frac{\mu_t}{Pr_t}\frac{\partial T}{\partial x_j} \tag{3}$$

In Equation (3), T represents temperature, λ is the thermal conductivity and Pr denotes the dimensionless Prandtl number. The Realizable k-ε, which is appropriate for the impingement jet and shear flow, is applied, whose equations are given by

$$\frac{\partial}{\partial x_j}\left(\rho \mathrm{k} u_j\right) = \frac{\partial}{\partial x_j}\left[\left(\mu + \frac{\mu_t}{\sigma_{\mathrm{k}}}\right)\frac{\partial \mathrm{k}}{\partial x_j}\right] + G_k + G_b - \rho\varepsilon - Y_{\mathrm{M}} + S_{\mathrm{k}} \tag{4}$$

$$\frac{\partial}{\partial x_j}\left(\rho \varepsilon u_j\right) = \frac{\partial}{\partial x_j}\left[\left(\mu + \frac{\mu_t}{\sigma_{\varepsilon}}\right)\frac{\partial \varepsilon}{\partial x_j}\right] + \rho C_1 S_{\varepsilon} - \rho C_2 \frac{\varepsilon^2}{k + \sqrt{\upsilon\varepsilon}} + C_{1\varepsilon}\frac{\varepsilon}{k} C_{3\varepsilon} G_b + S_{\varepsilon} \tag{5}$$

In these equations, G_k indicates the rate of turbulent kinetic energy production due to mean velocity gradients, and G_b represents the rate of turbulent kinetic energy production due to

buoyancy. Moreover, Y_M signifies the overall dissipation rate due to turbulence caused by compression, while the constants C_1 and C_2 are fixed. The terms σ_k and σ_ε are the turbulent Prandtl numbers for k and ε, respectively. The terms S_k and S_ε are source terms.

In this study, the Reynolds number is a significant independent variable. It will be calculated using the following equation

$$Re = \frac{\rho \times V \times D}{\mu} \quad (4)$$

where V is the inlet velocity, and D is the nozzle diameter. By assuming a specific value for the Reynolds number, the inlet velocity can be determined. Another important dimensionless variable in this problem is the Nusselt number. However, considering the shape and type of the problem, the Nusselt number will be calculated using the following equation

$$Nu = \frac{\dot{q} \times L}{\lambda \times (T_W - T_{inlet})} \quad (5)$$

In Equation (7), Nu represents the Nusselt number, $\dot{q}$ is the heat flux per unit area on the absorber plate, D is the jet diameter, T_W is the wall temperature, and T_{inlet} is the inlet fluid temperature.

One of the key variables in elucidating the hydrodynamic performance of the current geometry is the friction factor, which can be calculated using the following formula

$$f = \frac{1}{2 \times \rho \times V^2} \times D \times \frac{\Delta P}{L} \quad (6)$$

where f denotes the friction factor, and ΔP is the pressure drop within the channel. Finally, after calculating the Nusselt number and the friction factor, one can obtain the thermo-hydraulic performance parameter, referred to as performance evaluation criteria (PEC) in the literature. An increase in this index indicates that the rate of heat transfer surpasses the effects of friction. This variable is derived from the following relationship [31,32].

$$PEC = \frac{Nu/Nu_s}{(f/f_s)^{1/3}} \quad (7)$$

To solve the problem numerically, certain assumptions are necessary for a smoother resolution, which are outlined below.

- The flow is steady and incompressible.
- The fluid is Newtonian.
- The flow is turbulent within a Reynolds number range of 10,000 to 25,000.
- Gravitational effects and buoyancy forces are neglected, owing to the weak strength of the natural convection compared to the forced convection.
- Radiative heat transfer is disregarded, due to low temperature in the problem.
- Viscous losses are ignored.

2-3. Boundary Conditions and Thermo-Physical Properties

All solid surfaces are considered to have no-slip hydrodynamic conditions. Regarding the thermal boundary conditions of the walls, all are adiabatic except for the absorber, which is characterized by a thermal flux of 1000W/m², similar to Ref. [16]. The inlet velocity of the jet ranges from 24.34 to 121.72m/s, determined using the Reynolds number, while the gauge outlet pressure is fixed at zero, indicating fluid discharge to the ambient environment. The fluid used in this study is assumed to be air at a temperature of 300K, entering the channel through the impinging jets. All walls and jets are assumed to be made of aluminum. The properties of the air are reported in Table 2.

Table 2. The thermo-physical properties of the air

Property (unit)	value
Density (kg/m3)	1,192
Thermal conductivity (W/mK)	0.026
Specific heat capacity (kJ/kgK)	1,006
Dynamic viscosity (kg/ms)	1.849e-05

3. Numerical Simulation, Grid Independency and Verification

In the present study, the discretization of the momentum and energy equations is performed using third-order approximation. Due to the presence of pressure gradients, the PRESTO! method is employed for pressure calculations. Additionally, the SIMPLE algorithm is used to couple the velocity and pressure fields. The under-relaxation factors for pressure, density, momentum, turbulent kinetic energy, turbulent energy dissipation, and total energy are set at 0.3, 1.0, 0.7, 0.8, 0.8, and 1.0, respectively. Convergence is achieved when the residuals of energy and other equations fall below specified thresholds.

An adaptive meshing method has been employed for the current geometry, as it provides superior mesh quality compared to other techniques. Additionally, fine and dense cells using a boundary layer mesh are used near the jet walls to enhance the accuracy of flow calculations in regions with high gradients. This approach increases the precision of the calculations related to fluid flow as it enters the channel and reduces the Y+ values in the cell layers adjacent to the walls to the range that it should be for the standard wall function. Fig. 2 shows meshing in various parts of the geometry.

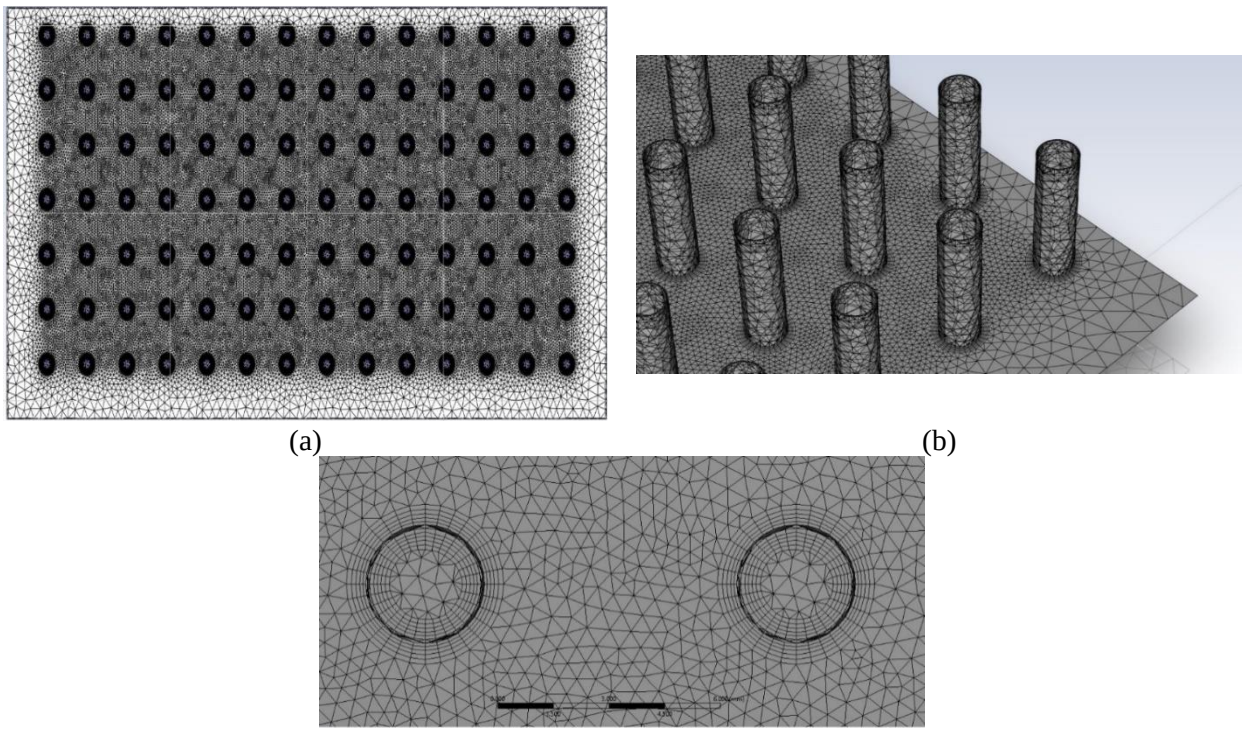

Fig. 2. The mesh generated in (a) The bottom plate of the solar heater, (b) Cells in the solid walls of the jets and (c) Boundary layer cells on the jets

To ensure the accuracy of the obtained results, it is essential to conduct a grid independence study. In the present research, the Nusselt number is calculated for various meshes at a jet diameter ratio of $\frac{D_j}{D_h}$=0.1042, a jet height ratio of $\frac{H_j}{D_h}$=0.2866, and a turbulence intensity of 5% at a Reynolds number of 20,000. These values have been compared as shown in the table below. Based on the results, the mesh with 2,095,693 computational cells has been selected as the optimal and most accurate mesh for this study.

Table 3. The grid independence test results

Cell numbers	Nusselt number	Relative error (%)
988,533	381.85	-
1,368,105	385.42	3.49
1,735,981	393.54	2.47
2,095,693	394.90	0.32
2,540,693	394.98	0.13

Before conducting the numerical simulations in this study, the current results were compared with those earlier published by Afroz and Sharif [33], which numerically investigated a symmetrically impinging jet. In their numerical research, fluid flow impinging on an absorber plate was investigated in a turbulent flow regime with Reynolds numbers ranging from 5,000 to 25,000. They calculated the Nusselt number by varying the diameter of a jet in several stages. As observed in Fig. 3, the differences between the obtained results are low. The variation in results at the lowest Reynolds number was 4%, and at the highest Reynolds number, it was 1%. This minor discrepancy is primarily attributed to the use of different discretization methods for the equations. Given this negligible difference, the results obtained in this study can be considered reliable.

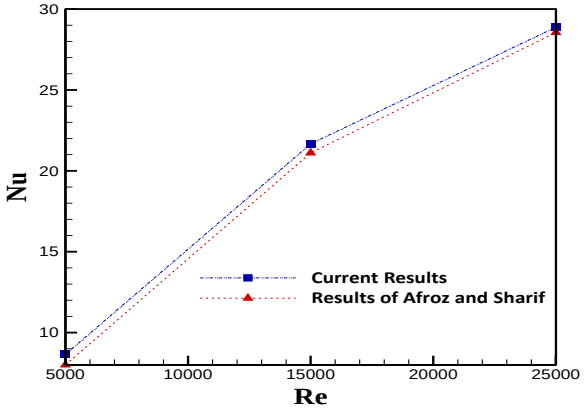

Fig. 3. A comparison between the current results and those derived by Afroz and Sharif [33]

4. Results and Discussions

In this section, the relationships between the variations of independent and dependent variables

are illustrated. The ranges of the independent variables are introduced in Table 4. The Nusselt number, friction factor, and PEC index are the dependent variables.

Table 4. The independent variables and ranges

Independent value	Range of variation
Reynolds number	10000 to 25000
The jets diameter ratio (D_j/D_h)	0.0781 to 0.176
The jets height ratio (H_j/D_h)	0 to 0.2866
The turbulence intensity	5% and 10%

4-1. The Baseline Case

Before addressing the comparison and presentation of the results for the current problem, it is essential to define the baseline geometry, which will also be referenced in the calculations. All obtained results are compared against this baseline. The baseline refers to the case of a simple channel functioning as a solar heater without impinging jets. Fig. 4 displays the results for the Nusselt number and friction factor in the baseline case.

As shown in Fig. 4, increasing the Reynolds number in the simple channel, which corresponds to higher inlet fluid velocity, leads to an almost linear increase in the Nusselt number. Furthermore, it makes an increment in the Nusselt number. The higher cost of the system by increasing the inlet velocity should keep in mind, as well. Additionally, raising the inlet turbulence intensity from 5% to 10% results in a negligible increase in the Nusselt number. It is important to consider specific scenarios where this factor may be more critical, such as in high flow rate applications or complex geometries. Further exploration of turbulence intensity under varying conditions could provide valuable insights for optimizing heat transfer in practical applications.

Regarding the friction factor, it decreases with an increase in the Reynolds number, but not in a strictly linear manner. Beyond a Reynolds number of 15,000, the rate of decrease in the friction factor diminishes, and the reduction becomes less significant as the Reynolds number increases past 15,000. While increasing the Reynolds number results in higher inlet fluid velocity, it also leads to increased pressure drop, which is undesirable and contributes to a higher friction factor, in spite of increasing the inlet velocity.

4-2. General Description of Temperature and Pressure Variations

Temperature contours are crucial for addressing thermal issues. Fig. 5a presents temperature contours for both the highest and lowest Nusselt numbers, with a height ratio of 0.2866, diameter ratio of 0.0781, turbulence intensity of 5%, and a fluid inlet velocity characterized by a Reynolds number of 25,000. The optimal location for displaying temperature contours is the hot surface, specifically the absorber, as it experiences the most significant temperature changes, making cooling variations readily apparent. According to the figure, the maximum temperature on the absorber plate reaches 304.2K, with cooler regions clearly identified. The cold spots occur on the plate facing the jet inlets, and the temperature difference across the plate is minimal at 4K, indicating nearly uniform cooling. Fig. 5b shows the temperature contours for the case with the lowest Nusselt number, associated with a diameter ratio of 0.1042, height ratio of zero, Reynolds number of 10,000, and turbulence intensity of 10%. In this scenario, the cold spots are more diffuse, and the temperature difference increases to over 20K. This indicates a reduction in both the strength and uniformity of cooling compared to the previous case.

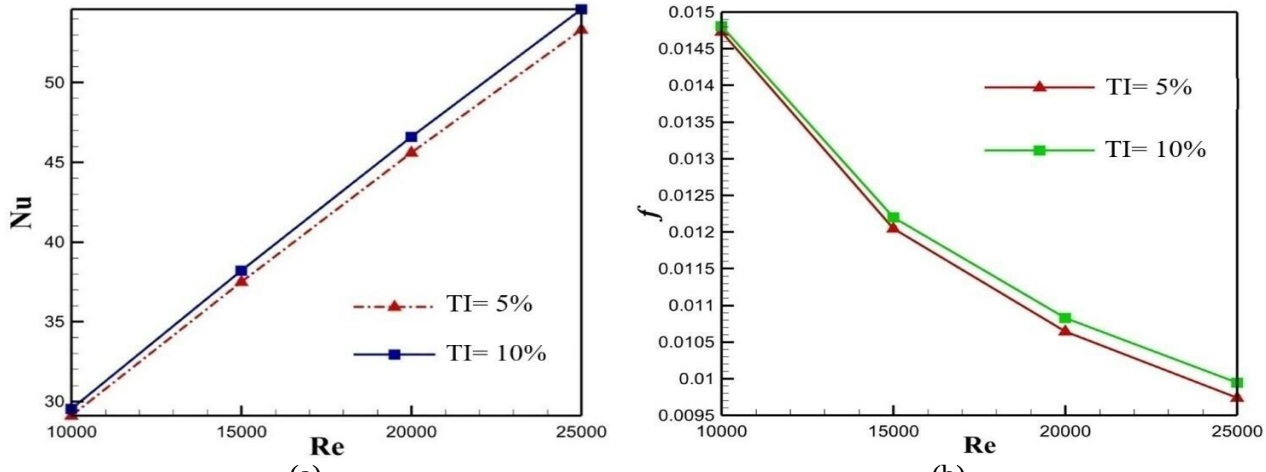

(a) (b)

Fig. 4. The variations of (a) Nusselt number and (b) Friction factor for the baseline case in two turbulence intensity values

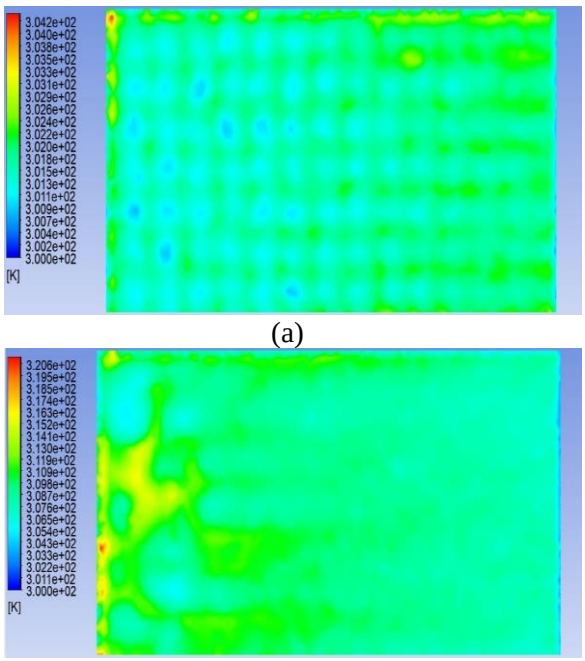

Fig. 5. Temperature contour on the absorber plate for (a) The case with the highest and (b) The lowest value of the Nusselt number.

Table. 6a shows the pressure contour on the symmetry plane of the case with highest friction factor, corresponding to diameter ratio of 0.0781, height ratio of 0.2866, Reynolds number of 10000 and turbulent intensity of 10%. The pressure decreases toward the outlet, which is owing to the outlet boundary conditions. The effect of the impingement jets is more apparent compared to the case with the lowest friction factor, shown in Fig. 4b, for diameter ratio of 0.156, the height ratio of zero, Reynolds number of 250000 and turbulence intensity of 5%. The changes in the flow pressure during journey in the channel is more uniform in Fig. 6b.

4-3. Impact of Jet Height Variation

In this section, the jet diameter is fixed at 6mm, while variations in Reynolds number and jet height are examined and compared. The results for the diameter ratio of 0.156 are shown in Fig. 7. As illustrated in subfigure (a), the Nusselt number increases linearly with rising Reynolds number. For instance, in a sample with a height ratio of 0.2866, increasing the Reynolds number from 10,000 to 25,000 raises the Nusselt number from 250 to 485, indicating a 94% increase. This rise in the Nusselt number is logical, as increasing the Reynolds number also increases the inlet fluid velocity through the jets, leading to a higher convective heat transfer. Additionally, it can be found that as the height ratio increases, the Nusselt number also rises. At a Reynolds number of 10,000, increasing the height ratio from 0 to 0.2866 raises the Nusselt number from 150 to 250, a 66% increase. This increase is attributed to the reduced distance between the fluid entry and the hot surface as the height ratio rises, resulting in enhanced cooling.

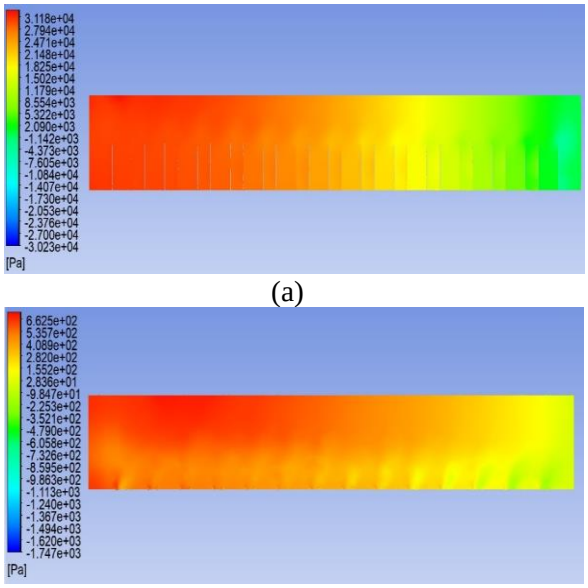

Fig. 6. Pressure contour on the symmetry plane for (a) The case with the highest and (b) The lowest value of the friction factor.

At a height ratio of 0.2866, the jets extend to half the height of the channel, which minimizes the distance among the cases studied and shows the best cooling performance with the highest Nusselt number. At higher Reynolds numbers, the impact of height ratio on cooling becomes more pronounced; for a Reynolds number of 10,000, the difference in Nusselt number between the maximum and minimum height ratios is 100. However, as the Reynolds number increases to 25,000, this difference rises to at least 160, indicating the significant role of the jet height ratio in higher Reynolds number ranges. Fig. 4b outlines the friction factor; it is evident that the friction factor decreases almost linearly with increasing Reynolds number. This decrease results from the increased inlet fluid velocity into the channel, which raises the denominator of the friction factor. However, higher Reynolds numbers also result in greater pressure drops within the channel, leading to a less steep decrease in the friction factor. Nevertheless, the increase in fluid velocity has a more significant effect than the pressure drop, resulting in a reduction in the friction factor.

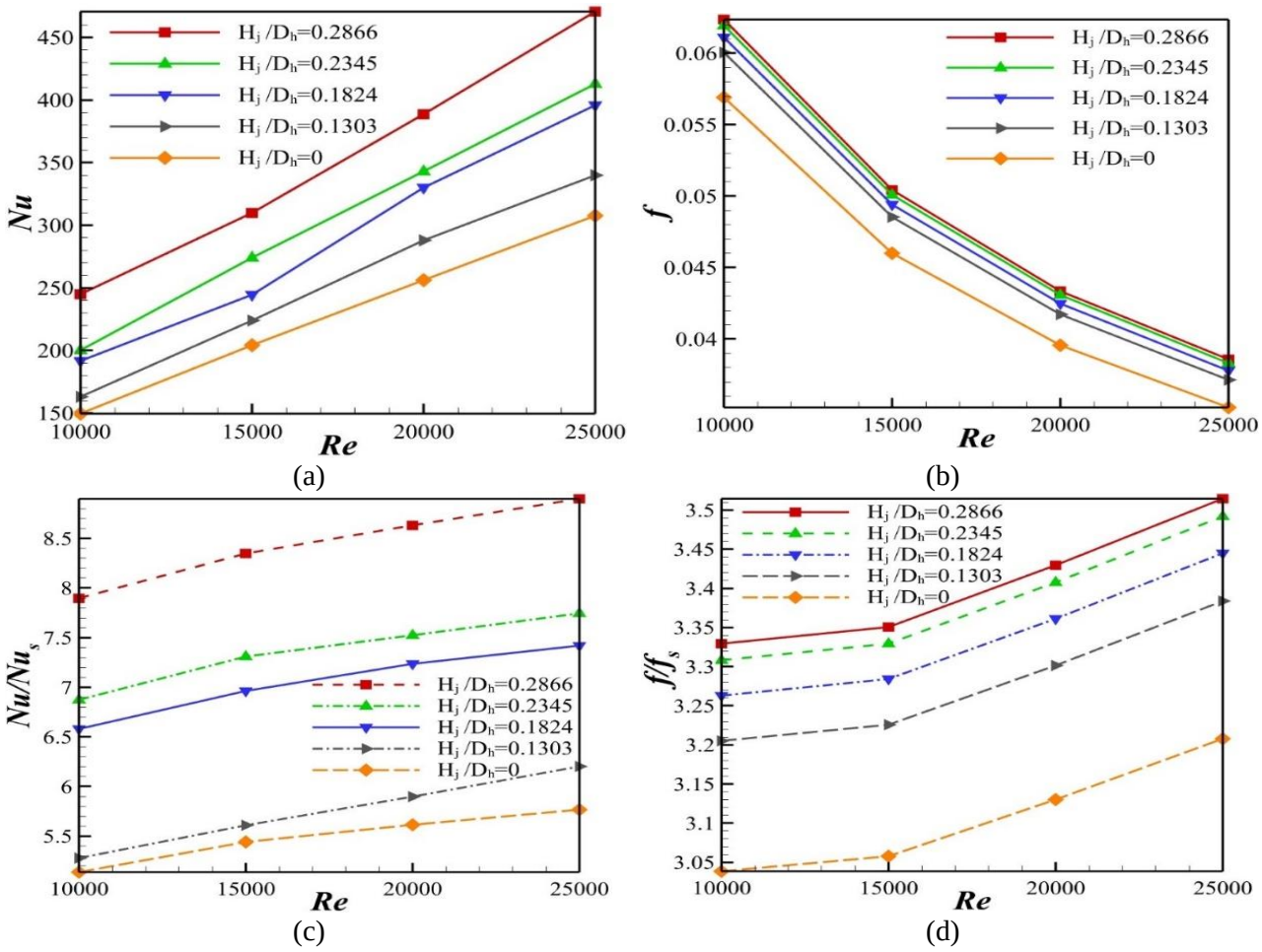

Fig. 7. Changes in (a) Nusselt number, (b) Friction factor, (c) Ratio of Nusselt number to baseline Nusselt number, and (d) Ratio of friction factor to baseline friction versus the Reynolds number at a diameter ratio of 0.156.

It is noted that the variation in height ratio across different cases does not significantly affect the friction factor. This can be due to the constant fluid velocity, resulting in only minor effects from height ratio changes on the pressure drop. Figs. 4c and 4d present values relative to the baseline condition, demonstrating how the use of impinging jets at the bottom of the solar heaters significantly improves the results. It can be seen that as the Reynolds number increases, the ratio of the Nusselt number to the baseline Nusselt number also rises, with height ratio changes significantly affecting this variable. The differences between various height ratios become more pronounced, indicating the beneficial impact of jets compared to the baseline solar heaters.

The ratio of the friction factor to the baseline friction factor also increases with higher Reynolds numbers. When the flow exceeds a Reynolds number of 15,000, a sudden increase occurs, highlighting the importance of flow velocity's effect on this variable. The difference between the zero height ratio and the maximum height ratio is noteworthy, as there is a considerable gap between these variables for the maximum and minimum height ratios. Thus, the height of the impinging jets plays a crucial role in enhancing the performance of the baseline solar heaters.

Fig. 8 indicates the PEC variations against Reynolds number. As noted, an increase in Reynolds number, which corresponds to higher fluid velocity, consistently enhances the overall system performance across all cases. The PEC increases almost linearly with rising Reynolds number; however, the effect of Reynolds number on the PEC is less significant than that of changes in jet height. An increase in height ratio is associated with an increase in the PEC. This is primarily due to the more rapid improvement of the Nusselt number relative to the friction factor compared to a flat surface.

4-4. Impact of Jet Diameter Variation

In this section, the height ratios are fixed, and the effects of diameter ratios are compared. The maximum jet height ratio of 0.2866, corresponding to a height of 11mm, is displayed, and various

diameter ratios are compared under this condition. Fig. 9a presents that the Nusselt number increases linearly with the Reynolds number, rising from 10,000 to 25,000. At a jet diameter ratio of 0.0781 and a height ratio of 0.2866, the Nusselt number is 225 at a Reynolds number of 10,000 and increases to 498 at 25,000. A notable point in this graph is the difference between the jet diameter ratios of 0.156 and 0.0781. As the Reynolds number increases, reducing the jet diameter leads to improved cooling and subsequently increases the Nusselt number.

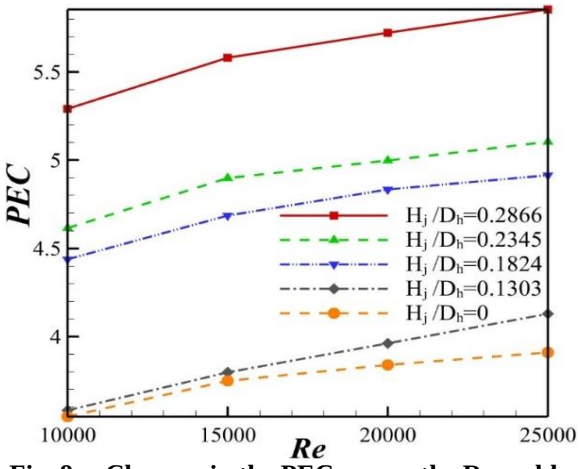

Fig. 8. Changes in the PEC versus the Reynolds number at the diameter ratio of 0.156.

Fig. 9b addresses changes in the friction factor variations. It is noted that the friction factor decreases almost uniformly with increasing Reynolds number. In this part, however, it is observed that increasing the jet diameter ratio from 0.0781 to 0.156 results in a reduction of the friction factor. As the jet diameter increases, the friction factor decreases across all height ratios. This reduction occurs because when the jet diameter decreases, the inlet fluid velocity increases at a constant Reynolds number, leading to a significant rise in pressure within the channel, which contributes to greater pressure drop, the primary factor behind the increased friction factor. While the increase in Reynolds number also boosts overall flow velocity and enhances cooling, it simultaneously reduces the friction factor.

Figs. 9c and 9d show the ratio of the Nusselt number to the baseline Nusselt number and the ratio of the friction factor to the baseline friction factor, respectively. Both metrics illustrate the changes in results obtained from solar heaters with impinging jets compared to simple solar heaters. The ratio of the Nusselt number increases with rising Reynolds number, which is entirely logical. However, it is noteworthy that the variations for the jet diameter ratios are not significant; the variables remains relatively constant with changes in jet diameter, with absolute differences reaching a maximum of 0.3, indicating that changes in the jet height ratio have a much greater impact on the Nusselt ratios than changes in jet diameter. Although the qualitative effect of jet diameter on the friction factor ratio is similar to the Nusselt number ratio, the impact of varying the jet diameter is more significant. Interestingly, the effect of Reynolds number and flow velocity on this variable is minimal; even at a Reynolds number of 25,000, the ratio of the friction factor increases by no more than 5%.

Fig. 6 illustrates the hydraulic-thermal performance index for this section. It can be observed that, similar to the effect of height ratio, an increase in Reynolds number is associated with an improvement in the PEC index. This improvement is attributed to the increased inlet fluid velocity, which ultimately leads to better cooling. As the diameter ratio increases from 0.0781 to 0.156, the PEC also rises. This indicates that although an increase in diameter ratio reduces the inlet fluid velocity and consequently leads to diminished cooling, it also results in lower pressure drops, which ultimately contributes to an increase in the PEC values.

4-5. Impact of Turbulence Intensity Variation

As explained, two turbulence intensity levels of 5% and 10% were considered in this study. For all earlier cases, however, the turbulence intensity was chosen as 5%. Fig. 11 illustrates the comparison between these two turbulence intensity levels. In spite of choosing the results from the case with the highest difference between two turbulence intensities, the figure illustrates a too small changes associated with variations in turbulence intensity. The subfigure (a) demonstrates that the difference in the Nusselt number between 5% and 10% turbulence intensity is minimal; for instance, at a diameter ratio of 0.156 and a Reynolds number of 25,000, the difference in the Nusselt number is less than 0.5%, a variation that can be considered negligible. Fig. 11b shows the PEC variation is illustrated. It is evident that there are no significant changes in the performance index when comparing results at 5% and 10% turbulence intensity. For example, at a diameter ratio of 0.156 and a Reynolds number of 25,000, the PEC index is approximately 5.6 at 5% turbulence intensity and drops to 4.9 at 10% turbulence intensity. This change is slight, and often the results are not even

discernible when plotted together. Despite these observations, it is noteworthy that increasing turbulence intensity has reduced the PEC index, indicating that the transition from 5% to 10% turbulence intensity has adversely affected PEC of the solar heater.

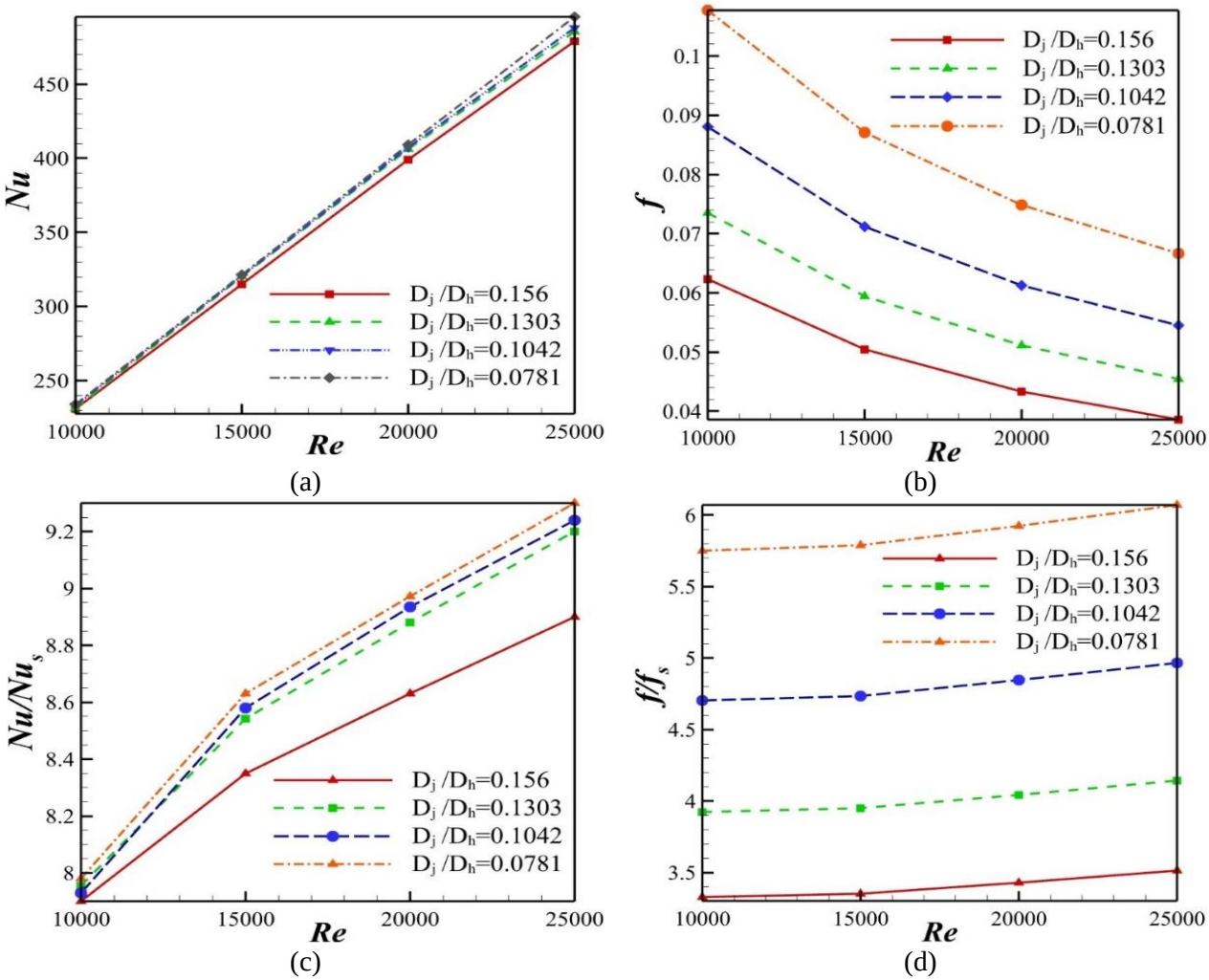

Fig. 9. Changes in (a) Nusselt number, (b) Friction factor, (c) Ratio of Nusselt number to baseline Nusselt number, and (d) Ratio of friction factor to baseline friction versus the Reynolds number at a height ratio of 0.2866.

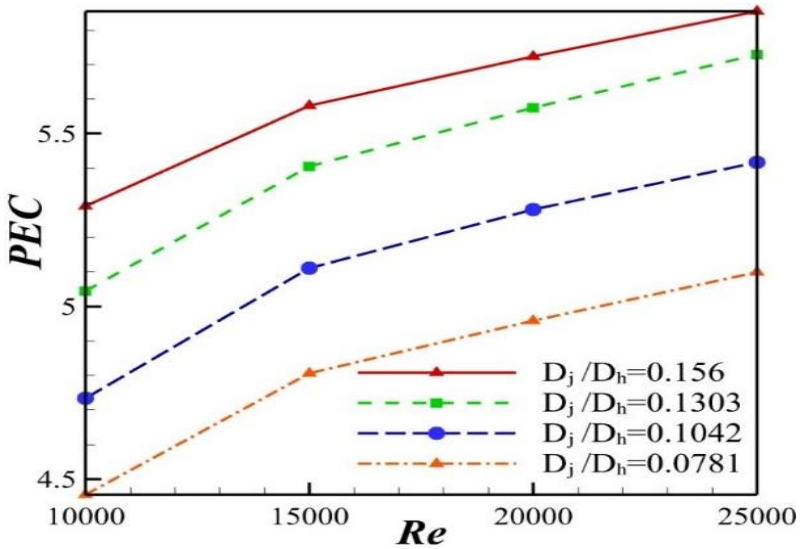

Fig. 10. Changes in the PEC at the height ratio of 0.2866.

Turbulence Intensity=10% Turbulence Intensity=5%

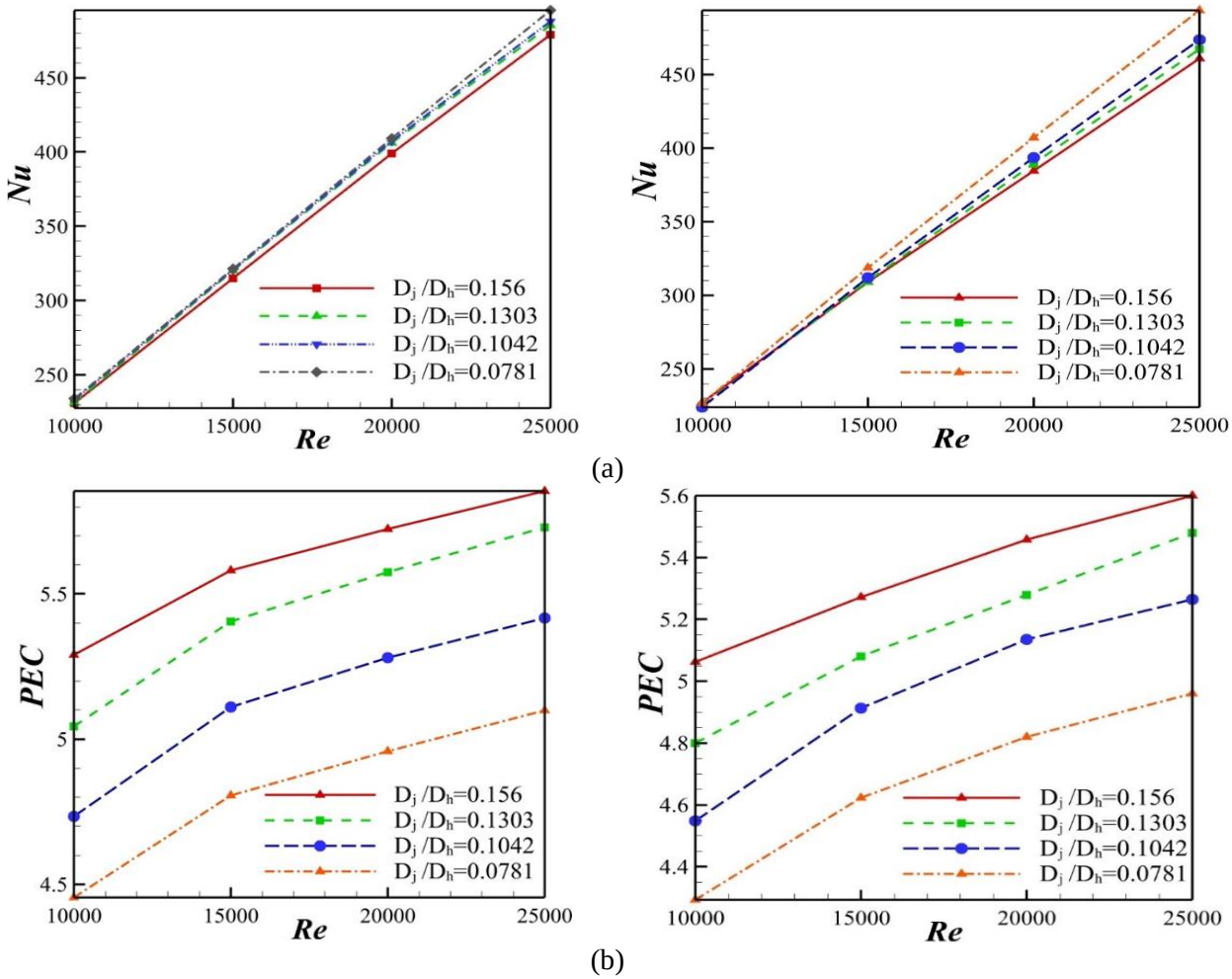

Fig. 11. Changes in (a) Nusselt number, and (b) PEC for two values of turbulent intensity of 5% and 10% at a height ratio of 0.2866.

5. Conclusion

This study investigated the effects of various parameters on the thermal performance of a solar heater, focusing on the Nusselt number, friction factor, and hydraulic-thermal performance, introduced by PEC. By varying the Reynolds number, turbulence intensity, height ratio, and diameter ratio, it was identified the configurations that significantly improve heat transfer and friction factor. The main findings of the current work are presented in the following.

- The results indicate that when turbulence intensity was set at 5%, the Reynolds number at 25,000, the height ratio at its maximum of 0.2866, and the diameter ratio at its minimum of 0.0781, the highest Nusselt number achieved was 495.44. This represented a ninefold increase compared to the baseline and a 4.5-fold increase compared to the minimum Nusselt number with the impinging jet.
- The minimum friction factor was noted when the Reynolds number and turbulence intensity were 25,000 and 5%, respectively, with a diameter ratio of 0.156 and a height ratio of zero, indicating an increase of approximately 1.8 times compared to the baseline.
- The PEC reached its lowest value of 1.986 under conditions of a Reynolds number of 10,000, turbulence intensity of 10%, a diameter ratio of 0.0781, and a height ratio of zero. This result demonstrated that even at minimal performance improvement, the studied solar heater outperformed baseline design. The highest PEC of 5.82 was achieved with a Reynolds number of 25,000, turbulence intensity of 5%, a diameter ratio of 0.156, and a height ratio of 0.2866.
- Keeping other independent variables constant and increasing the Reynolds number from 10,000 to 25,000 resulted in a 118.2% increase in Nusselt number, clearly illustrating the direct impact of Reynolds number on cooling efficiency. Additionally, increasing the Reynolds number improved the friction factor by 5% compared to the baseline, and the PEC

increases by 17%.

- Changing the height ratio from minimum to maximum led to an 85.7% increase in Nusselt number, a 33% rise in the friction factor compared to the baseline, and a 66% increase in the PEC.
- Similarly, adjusting the diameter ratio from minimum to maximum improved the Nusselt number by 5% while reducing the friction factor ratio by 41.6%, resulting in a 14% increase in the hydraulic-thermal performance index.
- Comparisons of results for turbulence intensity changes from 5% to 10% show only minor reductions in the evaluated variables.
- Drawing upon the insights gained from this study, it is recommend that future solar heater designs prioritize the optimization of jet height and diameter ratios to maximize thermal performance. By adopting these design principles, engineers and researchers can substantially improve the efficacy of solar heating systems in practical implementations, thereby advancing the adoption of renewable energy technologies.

References

[1] Nadda, R., Kumar, A., & Maithani, R. (2018). Efficiency improvement of solar photovoltaic/solar air collectors by using impingement jets: A review. *Renewable and Sustainable Energy Reviews*, *93*, 331-353.

[2] El-Bialy, E., & Shalaby, S. M. (2023). Recent developments and cost analysis of different configurations of the solar air heaters. *Solar Energy*, 112091.

[3] Chaurasia, S., Goel, V., & Debbarma, A. (2023). Impact of hybrid roughness geometry on heat transfer augmentation in solar air heater: A review. *Solar Energy*, *255*, 435-459.

[4] Aboghrara, A. M., Baharudin, B. T. H. T., Alghoul, M. A., Adam, N. M., Hairuddin, A. A., & Hasan, H. A. (2017). Performance analysis of solar air heater with jet impingement on corrugated absorber plate. *Case studies in thermal engineering*, *10*, 111-120.

[5] Nadda, R., Kumar, A., & Maithani, R. (2017). Developing heat transfer and friction loss in an impingement jets solar air heater with multiple arc protrusion obstacles. *Solar Energy*, *158*, 117-131.

[6] Barewar, S. D., Joshi, M., Sharma, P. O., Kalos, P. S., Bakthavatchalam, B., Chougule, S. S., ... & Saha, S. K. (2023). Optimization of jet impingement heat transfer: A review on advanced techniques and parameters. *Thermal Science and Engineering Progress*, *39*, 101697.

[7] Uddin, N., Kee, P. T. W., & Weigand, B. (2024). Heat transfer by jet impingement: A review of heat transfer correlations and high-fidelity simulations. *Applied Thermal Engineering*, 124258.

[8] Ewe, W. E., Fudholi, A., Sopian, K., Solomin, E., Yazdi, M. H., Asim, N., ... & Abimanyu, H. (2022). Jet impingement cooling applications in solar energy technologies: Systematic literature review. *Thermal Science and Engineering Progress*, *34*, 101445.

[9] Barbosa, F. V., Teixeira, S. F., & Teixeira, J. C. (2023). Convection from multiple air jet impingement-A review. *Applied Thermal Engineering*, *218*, 119307.

[10] Zukowski, M. (2013). Heat transfer performance of a confined single slot jet of air impinging on a flat surface. *International Journal of Heat and Mass Transfer*, *57*(2), 484-490.

[11] Ichimiya K (1995). Heat Transfer and Flow Characteristics of an Oblique Turbulent Impinging Jet Within Confined Walls. *Heat Transfer*, *117*, 316–22.

[12] Lin, Z. H., Chou, Y. J., & Hung, Y. H. (1997). Heat transfer behaviors of a confined slot jet impingement. *International Journal of Heat and Mass Transfer*, *40*(5), 1095-1107.

[13] Huang, X. Q., Leung, C. W., Chan, C. K., & Probert, S. D. (2006). Thermal characteristics of a premixed impinging circular laminar-flame jet with induced swirl. *Applied energy*, *83*(4), 401-411.

[14] Chauhan, R., & Thakur, N. S. (2013). Heat transfer and friction factor correlations for impinging jet solar air heater. *Experimental Thermal and Fluid Science*, *44*, 760-767.

[15] Zukowski, M. (2015). Experimental investigations of thermal and flow characteristics of a novel microjet air solar heater. *Applied Energy*, *142*, 10-20.

[16] Yadav, S., & Saini, R. P. (2020). Numerical investigation on the performance of a solar air heater using jet impingement with absorber plate. *Solar Energy*, *208*, 236-248.

[17] Metzger, L., & Kind, M. (2016). On the mixing in confined impinging jet mixers–Time scale analysis and scale-up using CFD coarse-graining methods. *Chemical Engineering Research and Design*, *109*, 464-476.

[18] Ingole, S. B., & Sundaram, K. K. (2016). Experimental average Nusselt number characteristics with inclined non-confined jet impingement of air for cooling application. *Experimental Thermal and Fluid Science*, *77*, 124-131.

[19] Nayak, R. K., & Singh, S. N. (2016). Effect of geometrical aspects on the performance of jet plate solar air heater. *Solar Energy*, *137*, 434-440.

[20] Rajaseenivasan, T., Prasanth, S. R., Antony, M. S., & Srithar, K. (2017). Experimental investigation on the performance of an impinging jet solar air heater. *Alexandria Engineering Journal*, *56*(1), 63-69.

[21] Lam, P. A. K., & Prakash, K. A. (2017). A numerical investigation and design optimization of impingement cooling system with an array of air jets. *International Journal of Heat and Mass Transfer*, *108*, 880-900.

[22] Singh, S., Chaurasiya, S. K., Negi, B. S., Chander,

S., Nemś, M., & Negi, S. (2020). Utilizing circular jet impingement to enhance thermal performance of solar air heater. *Renewable energy*, *154*, 1327-1345.
[23] Zhu, K., Yu, P., Yuan, N., & Ding, J. (2018). Transient heat transfer characteristics of array-jet impingement on high-temperature flat plate at low jet-to-plate distances. *International Journal of Heat and Mass Transfer*, *127*, 413-425.
[24] Zhu, K., Yu, P., Yuan, N., & Ding, J. (2018). Transient heat transfer characteristics of array-jet impingement on high-temperature flat plate at low jet-to-plate distances. *International Journal of Heat and Mass Transfer*, *127*, 413-425.
[25] Alomar, O. R., Abd, H. M., & Salih, M. M. M. (2022). Efficiency enhancement of solar air heater collector by modifying jet impingement with v-corrugated absorber plate. *Journal of Energy Storage*, *55*, 105535.
[26] Yadav, S., Saini, R. P., & Pandey, K. M. (2023). Effect of jet angle and jet pitch on the Thermo-Hydraulic performance of solar air heater having absorber plate with jet impingement. *Thermal Science and Engineering Progress*, *45*, 102146.
[27] Hai, T., Mansir, I. B., Alshuraiaan, B., Abed, A. M., Ali, H. E., Dahari, M., & Albalawi, H. (2023). Numerical investigation on the performance of a solar air heater using inclined impinging jets on absorber plate with parallel and crossing orientation of nozzles. *Case Studies in Thermal Engineering*, *45*, 102913.
[28] Almeshaal, M., Palaniappan, M., & Matheswaran, M. M. (2024). Assessment and enhancement of thermal performance for ring roughened finned jet impingement solar air heater for low-temperature applications. *Energy*, *307*, 132632.
[29] Harikrishnan, M., Kumar, R. A., Baby, R., Percy, D., & Kumar, S. A. (2024). Exergetic performance assesment of a downward solar air heater with impinging air jets-An experimental study. *Case Studies in Thermal Engineering*, *55*, 104104.
[30] Elwekeel, F. N., Nasr, A. A. E., Radwan, M. I., & Aly, W. I. (2024). Influence of impingement jet designs on solar air collector performance. *Renewable Energy*, *221*, 119757.
[31] Yilmaz, M., Sara, O. N., & Karsli, S. (2001). Performance evaluation criteria for heat exchangers based on second law analysis. *Exergy, an International Journal*, *1*(4), 278-294.
[32] Webb, R. L., & Eckert, E. R. G. (1972). Application of rough surfaces to heat exchanger design. *international journal of heat and mass transfer*, *15*(9), 1647-1658.
[33] Afroz, F., & Sharif, M. A. (2018). Numerical study of turbulent annular impinging jet flow and heat transfer from a flat surface. *Applied Thermal Engineering*, *138*, 154-172.

Biography

Mehdi Ashja is a PhD student in Mechanical Engineering, specializing in Energy Conversion, at University of Kashan. He completed his MSc in 2021 at the same institution. Passionate about renewable energy, numerical simulations, solar energy, and the integration of artificial intelligence and machine learning, Mehdi's research is focused on developing innovative solutions to advance sustainable energy technologies.

Ghanbar Ali Sheikhzadeh is a Professor in the Faculty of Mechanical Engineering and the Energy Research Institute at the University of Kashan. He earned his PhD in Mechanical Engineering with a focus on Energy Conversion from Shahid Bahonar University of Kerman. With over 22 years of academic experience at the University of Kashan, Professor Sheikhzadeh teaches both undergraduate and graduate courses in heat transfer and computational fluid dynamics. He has supervised numerous students in the areas of thermal systems and heat transfer, and has published extensively in leading academic journals.

Abolfazl Fattahi is an Assistant Professor in the Faculty of Mechanical Engineering at the University of Kashan, specializing in energy conversion. He earned his PhD from Iran University of Science and Technology. In addition to fundamental research in fluid flow and heat transfer, his work focuses on energy systems and the sustainable development of energy utilization, incorporating machine learning techniques. Dr. Fattahi teaches courses in CFD and thermodynamics and has supervised numerous undergraduate and graduate students.

Najmeh Hajialigol is an Assistant Professor at Hamedan University of Technology. She earned her Ph.D. from Tarbiat Modares University in Mechanical Engineering, energy conversion. Dr. Hajialigol teaches courses in fluid mechanics, heat transfer, CFD and thermodynamics. Her research focuses on combustion, energy systems, and the application of machine learning to optimize integrated energy systems.